J. Fluid Mech. (2008), *vol.* 606, *pp.* 105–114. © 2008 Cambridge University Press
doi:10.1017/S0022112008001894 Printed in the United Kingdom

Thermal levitation

F. MANDUJANO AND R. RECHTMAN†

Centro de Investigación en Energía, Universidad Nacional Autónoma de México,
Apdo. Postal 34, 62580 Temixco, Mor., Mexico

(Received 31 January 2008 and in revised form 2 April 2008)

A particle with a density slightly larger than that of the fluid in which it is immersed will sediment. However, if the particle's temperature is higher than that of the fluid, the terminal velocity of sedimentation will be smaller and can even change sign. When the terminal velocity is zero we say there is thermal levitation. Thermal levitation can also occur when the density and temperature of the particle are smaller than those of the fluid. Using a two-component thermal lattice Boltzmann equation method, we study this phenomenon and show it can be stable or unstable.

1. Introduction

Circular particles moving in a two-dimensional Newtonian fluid have been studied numerically under diverse circumstances. Hu, Fortes & Joseph (1992*a*), Hu, Joseph & Crochet (1992*b*) and Feng, Hu & Joseph (1994) analysed the sedimentation of a particle in a narrow cavity by solving Navier–Stokes equations. Gan *et al.* (2003) and Yu, Shao & Wachs (2006) studied the case of a particle with constant temperature. Among other results, they found that the temperature difference has a significant effect on the terminal velocity of the particle and can even change the direction of motion.

We study the motion of a particle with a constant temperature in contact with a fluid in a narrow cavity with walls also at a constant temperature. The fluid is initially at the wall temperature. If the density and temperature difference between the particle and fluid are small, the buoyancy, drag and convective forces balance and the particle will move with a constant vertical terminal velocity. Thus, there is a thermal correction to Stokes' law. When the terminal velocity is zero, the convective force balances the buoyancy force and we call this state stable thermal levitation. As the temperature or density difference increase, thermal levitation becomes unstable.

To study a moving particle inside a fluid with heat transfer we used a D2Q9 (Qian, d'Humieres & Lallemand 1992) thermal two-component lattice Boltzmann equation (LBE) (Shan 1997; Inamuro *et al.* 2002). The boundary conditions for moving particles in isothermal flows using LBE were first proposed by Ladd (1994) and improved by Aidun & Lu (1995) and Aidun, Lu & Ding (1998). Guo & Zheng (2002) extended the algorithm to handle arbitrary geometries. The first boundary conditions for the temperature field were extensions of the bounce-back rule (Inamuro *et al.* 2002; Shan 1997) for flat walls and were generalized by Huang, Lee & Shu (2006) for walls of arbitrary shape using an interpolation method. In this paper, we extend the above boundary conditions to a moving particle with heat transfer.

In § 2 we briefly discuss the two-component thermal LBE method followed by a presentation of the flow of interest and validation of the method in § 3. In § 4 we

† Author to whom correspondence should be addressed: rrs@cie.unam.mx

https://doi.org/10.1017/S0022112008001894 Published online by Cambridge University Press

present numerical simulations of stable and unstable thermal levitation. We end with some conclusions in § 5.

2. LBE method

In order to numerically investigate the problem of the motion of a cylindrical particle in a fluid with thermal gradients, we used a D2Q9 two-component lattice Boltzmann equation which takes into account moving circular boundaries. In this method, space is two-dimensional and discretized using a square lattice. The state of the fluid at the node with vector position $\boldsymbol{r}$ at time t is described by the particle $f_k(\boldsymbol{r}, t)$ and temperature $g_k(\boldsymbol{r}, t)$ distributions that evolve in time and space according to

$$\tilde{f}_k(\boldsymbol{r}, t) = f_k(\boldsymbol{r}, t) - \frac{1}{\tau}\left[f_k(\boldsymbol{r}, t) - f_k^{(eq)}(\boldsymbol{r}, t)\right] + G_k, \tag{2.1}$$

$$f_k(\boldsymbol{r} + \boldsymbol{e}_k, t + 1) = \tilde{f}_k(\boldsymbol{r}, t), \tag{2.2}$$

$$\tilde{g}_k(\boldsymbol{r}, t) = g_k(\boldsymbol{r}, t) - \frac{1}{\tau_T}\left[g_k(\boldsymbol{r}, t) - g_k^{(eq)}(\boldsymbol{r}, t)\right], \tag{2.3}$$

$$g_k(\boldsymbol{r} + \boldsymbol{e}_k, t + 1) = \tilde{g}_k(\boldsymbol{r}, t). \tag{2.4}$$

The time evolution is conveniently divided in two steps: collision (relaxation towards local equilibrium) in (2.1) and (2.3) and streaming in (2.2) and (2.4). The collision step is local and the streaming is uniform. The coefficients τ and τ_T are the relaxation times related to the fluid viscosity ν and thermal diffusivity α by

$$\nu = (\tau - 1/2)/3, \qquad \alpha = (\tau_T - 1/2)/3.$$

The equilibrium distribution functions $f_k^{(eq)}$ and $g_k^{(eq)}$ are

$$f_k^{(eq)}(\boldsymbol{r}, t) = w_k \rho \left(1 + 3\boldsymbol{e}_k \cdot \boldsymbol{u} + \tfrac{9}{2}(\boldsymbol{e}_k \cdot \boldsymbol{u})^2 - \tfrac{3}{2}\boldsymbol{u}^2\right), \tag{2.5}$$

$$g_k^{(eq)}(\boldsymbol{r}, t) = w_k T(1 + 3\boldsymbol{e}_k \cdot \boldsymbol{u}). \tag{2.6}$$

In these expressions, the macroscopic fields are

$$\rho(\boldsymbol{r}, t) = \sum_k f_k(\boldsymbol{r}, t), \tag{2.7}$$

$$\rho \boldsymbol{u}(\boldsymbol{r}, t) = \sum_k \boldsymbol{e}_k f_k(\boldsymbol{r}, t), \tag{2.8}$$

$$T(\boldsymbol{r}, t) = \sum_k g_k(\boldsymbol{r}, t), \tag{2.9}$$

ρ, $\boldsymbol{u}$ and T being the density, velocity and temperature fields. The microscopic velocities $\boldsymbol{e}_k$ are given by

$$\begin{aligned}
&\boldsymbol{e}_0 = (0, 0),\\
&\boldsymbol{e}_k = (\cos(\pi(k-1)/2), \sin(\pi(k-1)/2)), \ k = 1, \ldots, 4,\\
&\boldsymbol{e}_k = \sqrt{2}\,(\cos(\pi(k-9/2)/2), \sin(\pi(k-9/2)/2)), \ k = 5, \ldots, 8,
\end{aligned}$$

and $w_0 = 4/9$, $w_k = 1/9$ for $k = 1, \ldots, 4$ and $w_k = 1/36$ for $k = 5, \ldots, 8$.

The last term in (2.1) is related to a body force which in this case is the Boussinesq approximation to the buoyancy force (Inamuro *et al.* 2002),

$$G_k = -3\beta w_k (T(\boldsymbol{r}, t) - T_w)\boldsymbol{e}_k \cdot \boldsymbol{g}, \tag{2.10}$$

https://doi.org/10.1017/S0022112008001894 Published online by Cambridge University Press

where β is the coefficient of thermal expansion, $\boldsymbol{g}$ is the acceleration due to gravity and T_w is a reference temperature chosen as the temperature of the cavity walls.

Clearly, (2.1)–(2.4) can be applied only if the neighbours of a fluid node are fluid. When a fluid node is near a solid wall, additional information must be provided. Half-way bounce–back boundary conditions were used for flat solid walls (Ladd 1994) for both the particle and temperature distribution functions. For curved walls the boundary conditions of Guo & Zheng (2002) were used for the particle distribution functions, and those of Huang *et al.* (2006) for the temperature distribution functions. In these cases, the unknown distribution functions at a solid node are separated into equilibrium and non-equilibrium parts. The first is calculated using a fictitious equilibrium function that enforces the boundary condition and the non-equilibrium part is approximated by that of the neighbouring fluid along the link using an interpolation scheme.

For any given time step the force and torque acting on the body are computed using the momentum-exchange method of Mei *et al.* (2002) and the new position of the particle is found using Newton's equation of motion. The particle moves continuously and every now and then it covers and uncovers some nodes. The covered nodes change from fluid to solid while those that are uncovered change from solid to fluid. Covered nodes assume the momentum of the fluid and there is a net force on the particle from all the covered nodes. Uncovered nodes assume the average density and temperature of all the neighbour fluid nodes and the velocity of the particle's boundary. There is also a net force on the particle. These two contributions are added to the force evaluated with the momentum-exchange method to find the total hydrodynamic force and torque on the particle. Since we know the density, momentum, and temperature of the uncovered nodes, their particle and temperature distribution functions can be found by assuming these nodes are in equilibrium and using (2.5) and (2.6).

To keep the particle inside the container, a bounce-back rule was implemented. When the distance between the particle and a wall is below some threshold, the particle's velocity normal to the wall is reversed. The results obtained show that this model is enough in sufficient the case when particle–wall collisions are rare.

3. Problem and validation

A narrow cavity of height H and width W with walls at a fixed temperature T_w is filled with a fluid that has an initial density ρ_f and temperature T_w. A cylindrical particle with diameter d, density ρ_p and fixed temperature T_p is released on the centreline of the cavity at some distance from the bottom. This is shown schematically in figure 1(*a*).

The non-dimensional position $\boldsymbol{r}^*$, time t^*, velocity $\boldsymbol{u}^*$, and force $\boldsymbol{F}^*$ are

$$\boldsymbol{r}^* = \frac{\boldsymbol{r}}{d}, \quad t^* = t\frac{\alpha}{d^2}, \quad \boldsymbol{u}^* = \boldsymbol{u}\frac{d}{\alpha}, \quad \boldsymbol{F}^* = \boldsymbol{F}\frac{d}{\rho_f \nu\alpha}.$$

The non-dimensional parameters that define the flow are $W^* = W/d$, $H^* = H/d$, and the Grashof number Gr, Prandtl number Pr, and density ratio σ given by

$$Gr = \frac{\rho_f^2 \beta \Delta T d^3 g}{\nu^2}, \quad Pr = \frac{\nu}{\alpha}, \qquad \sigma = \frac{\rho_p}{\rho_f},$$

https://doi.org/10.1017/S0022112008001894 Published online by Cambridge University Press

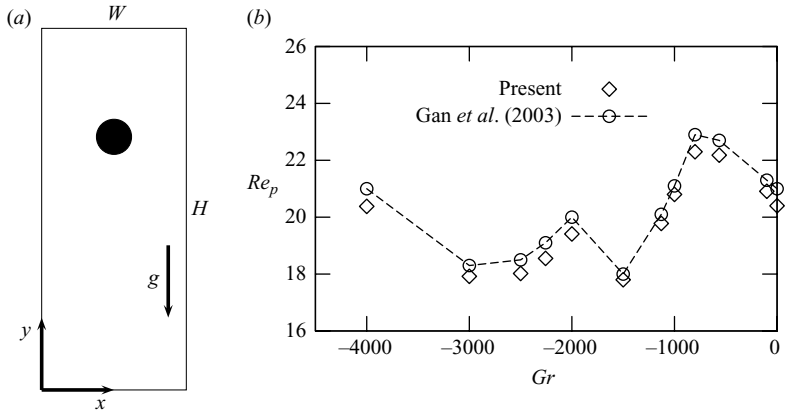


FIGURE 1. (*a*) A cylindrical particle inside a narrow cavity of width W and height H. (*b*) Comparison of the particle Reynolds number at different Grashof numbers for a particle with $\rho_p > \rho_f$ and $T_p < T_w$ settling in a vertical channel. The results of Gan *et al.* (2003) were with $(Pr, \sigma, W) = (7.0, 1.00232, 4)$ and $Re_p = 21$ when $Gr = 0$. In our simulations $(Pr, \sigma, W, H) = (0.7, 1.00232, 4, 60)$ and $Re_p = 20.4$ when $Gr = 0$.

where $\Delta T = T_p - T_w$. We note that $Gr > 0$ $(Gr < 0)$ when $T_p > T_w$ $(T_p < T_w)$. The particle Reynolds number Re_p is

$$Re_p = u_T \frac{d}{\nu},$$

where u_T is the particle's terminal velocity. In the following we always report our results in non-dimensional quantities and omit the asterisks.

We validated the code with various flows: natural and forced convection between concentric (Huang *et al.* 2006; Shu & Zhu 2002) and eccentric cylinders (Sadat & Couturier 2000) for a fixed particle, and sedimentation of a particle in a cavity with and without temperature gradients (Gan *et al.* 2003; Feng *et al.* 1994). In all cases, the results are in good agreement with those reported in the literature.

In particular, in figure 1(*b*) we compare our results of the particle Reynolds number for different Grashof numbers for the sedimentation of a particle with $\rho_p > \rho_f$ and $T_p < T_w$ with those of Gan *et al.* (2003) with $Re_p = 21$ when $Gr = 0$. Our results for Re_p with $Re_p = 20.4$ when $Gr = 0$ are slightly smaller and this difference can be attributed to the difference in the value of Re_p when $Gr = 0$ since the values reported by Yu *et al.* (2006) with $Re_p = 21.2$ for $Gr = 0$ are slightly larger than those of Gan *et al.* (2003). In these simulations we used $d = 25$ lattice sites and $H = 80$.

To study thermal levitation, we take $Pr = 7$, $W = 4$ and $d = 25$ lattice sites. The height of the cavity was varied from $H = 30$ to $H = 80$ and we found that the effects due to the top and bottom walls are negligible when $H \geqslant 40$ for small Re_p. Typical simulations require 10^6 iterations. Using an AMD Opteron processor the update time per site is 3×10^{-6} s so runs took approximately five days.

We will refer to a heavy (light) particle when $\sigma > 1$ $(\sigma < 1)$ and to a hot (cold) particle when $Gr > 0$ $(Gr < 0)$. Our main interest is to find Gr_0, the value of the Grashof number where $Re_p = 0$ and the particle levitates thermally.

https://doi.org/10.1017/S0022112008001894 Published online by Cambridge University Press

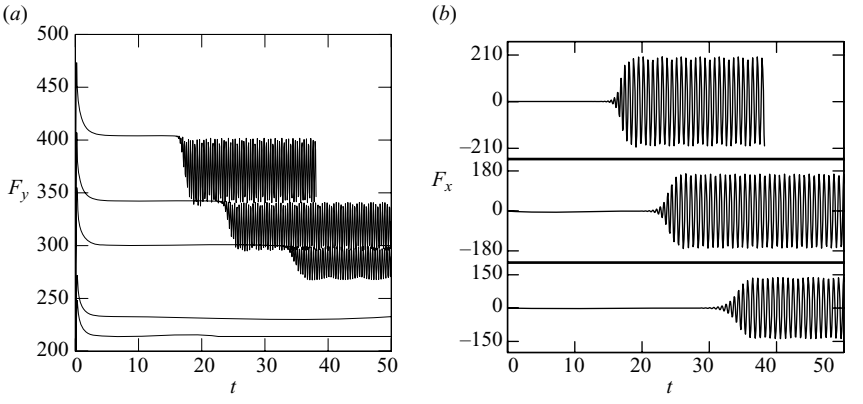


FIGURE 2. (*a*) The vertical component of the convective force F_y on a fixed particle as a function of time t. From bottom to top, $Gr = 50$, 54.3, 70, 80, and 95. (*b*) The horizontal component of the convective force F_x on a fixed particle as a function of time t. From bottom to top, $Gr = 70$, 80 and 95.

4. Results

We first consider a fixed particle initially on the axis of the cavity and measure the hydrodynamic force $\boldsymbol{F}$ on its surface as a function of the Grashof number. For a hot particle we find that after a small transient $\boldsymbol{F}$ reaches a steady state which is stable when Gr is smaller than a critical value $Gr_c^{(+)}$. In this stable steady state $F_x = 0$, and F_y grows linearly with Gr. For $Gr > Gr_c^{(+)}$ we find that after a small transient $F_x = 0$ and F_y reaches a constant value which after a time t_o yields to an oscillation of F_x and somewhat later of F_y as we show in figure 2. For a cold particle we found the same qualitative behaviour and another critical value $Gr_c^{(-)}$. In summary,

$$F = \begin{cases} C^{(+)}Gr, & 0 \leqslant Gr < Gr_c^{(+)}, \\ C^{(-)}Gr, & Gr_c^{(-)} < Gr \leqslant 0, \end{cases} \tag{4.1}$$

with $C^{(-)} < C^{(+)}$ constants. Larger values of the fluid velocity occur in regions where the temperature is higher, hence the force at a fixed value of $|Gr|$ is larger for a hot particle than for a cold one.

When $Gr > Gr_c^{(+)}$ the force on the particle oscillates after a transient t_o as we show in figure 2. We note that F_y oscillates with twice the frequency of F_x. Also, the amplitude of oscillation of F_x, A_x, grows and t_o decreases as $Gr - Gr_c^{(+)}$ grows:

$$A_x \sim (Gr - Gr_c^{(+)})^{\eta} \quad \text{and} \quad t_o \sim (Gr - Gr_c^{(+)})^{\xi}, \tag{4.2}$$

with $Gr_c^{(+)} = 53$, $\eta = 0.45$, and $\xi = -0.78$. For a cold particle $Gr_c^{(-)} = -65$, $\eta = 0.45$ and $\xi = -0.78$. We also find that the frequency of oscillation does not depend on $Gr - Gr_c^{(\pm)}$. These results indicate that there are Hopf supercritical bifurcations at $Gr_c^{(+)}$ and $Gr_c^{(-)}$ (Bérge, Pomeau & Vidal (1988); Desrayaud & Lauriat 1993). For F_y we find the same scaling behaviour for the time when the oscillation begins.

In figure 3(*a–d*) we show the evolution of the vorticity lines and in figure 3(*e–f*) the corresponding position of ideal tracers initially in three rings around the particle for $Gr = 95$ (the top curves in figure 2*a*, *b*). For $t < t_o$, (*a* and *e*), there is a steady flow with two vortices. When $t \gtrsim t_o$, (*b*), the vorticity lines begin to oscillate, the two vortices break into smaller ones and we observe vortex shedding. A vortex is formed on the left side of the particle, (*c*), which is shed as a new one is being formed, (*d*), and this

https://doi.org/10.1017/S0022112008001894 Published online by Cambridge University Press

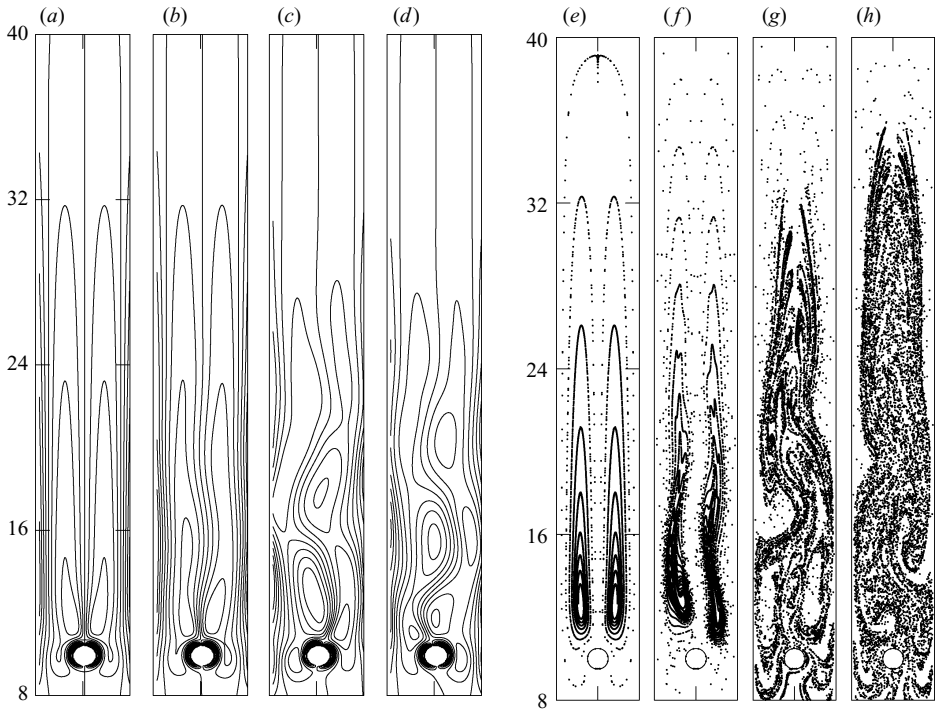


FIGURE 3. Isovorticity lines (*a*)–(*d*) and position of ideal tracers (*e*)–(*h*) for $Gr = 95$ for which $t_o = 13.5$. In (*a*) and (*e*) $t = 7.61$, in (*b*) and (*f*) $t = 16.38$, in (*c*) and (*g*) $t = 19.40$, and in (*d*) and (*h*) $t = 20.95$. There are 9000 ideal tracers initially located in three concentric rings around the particle, of diameters 1.16, 1.24 and 1.32.

process continues. The tracers show periodic orbits during the transient steady state, (*e*), and mixing for $t > t_o$ (*f*–*h*) (Ottino 1989).

A free particle initially on the axis of the cavity with σ slightly different from 1 will move vertically and after a transient reach a steady state with a positive, negative or zero terminal velocity u_T depending on the value of the Grashof number as we show in figure 4 where $u_T = 0$ when $Gr = 28$. We found numerically that

$$u_T = a(Gr - Gr_0), \tag{4.3}$$

where Gr_0 is the Grashof number for thermal levitation and a is a constant. Numerical results for different values of σ are shown in figure 5 in terms of the particle Reynolds number. The linear relation between the Grashof number and the terminal velocity holds when Gr is near the levitation value Gr_0 because the flow will be in the limit of low Reynolds numbers where Stokes' law holds.

When the particle reaches its terminal velocity the total force is zero so

$$C^{(\pm)}Gr + \frac{\pi d^3 g(1-\sigma)}{4\nu\alpha} - \delta u_T = 0, \tag{4.4}$$

where the first term is the convective force taken from (4.1), the second the buoyancy force and the last one Stokes' drag force (δ a constant). For thermal levitation, $u_T = 0$ and $Gr = Gr_0$ so that

$$Gr_0 = \frac{\pi d^3 g(\sigma - 1)}{4C^{(\pm)}\nu\alpha}. \tag{4.5}$$

https://doi.org/10.1017/S0022112008001894 Published online by Cambridge University Press

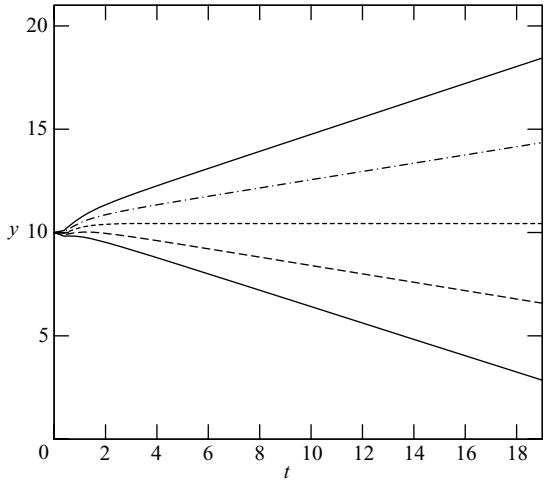


FIGURE 4. Vertical position of a hot heavy particle for different Grashof numbers with $H = 60$ and $\sigma = 1.005$. From bottom to top, $Gr = 26, 27, 28, 29$, and 30.

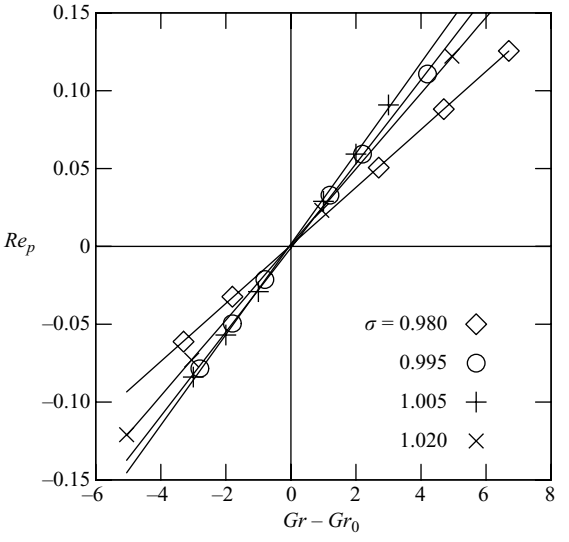


FIGURE 5. Particle Reynolds number Re_p as a function of $Gr - Gr_0$. For $\sigma = 0.98$ $Gr_0 = -114.5$, for $\sigma = 0.995$ $Gr_0 = -28.2$, for $\sigma = 1.005$ $Gr_0 = 28$ and for $\sigma = 1.02$ $Gr_0 = 110.2$. For $\sigma = 0.995$ and 1.005 thermal levitation is stable, and for the other values of σ thermal levitation is unstable.

This result is valid when $Gr_c^{(-)} < Gr_0 < Gr_c^{(+)}$. Outside this interval thermal levitation is unstable; after some time the particle begins to oscillate and migrates vertically. From the bounds on Gr for stable thermal levitation and (4.5), we find equivalently that if $\sigma_c^{(-)} < \sigma < \sigma_c^{(+)}$ with $\sigma_c^{(-)} \sim 0.99$ and $\sigma_c^{(+)} \sim 1.01$, thermal levitation is stable. This is confirmed in figures 6 and 7. In this case, instability sets in via a Hopf supercritical bifurcation as before.

For a hot heavy particle we show in figure 6 that thermal levitation is stable for $\sigma = 1.005$ and unstable for larger values where oscillations in both directions cause the particle to sink after a transient where the particle levitates. A similar behaviour

https://doi.org/10.1017/S0022112008001894 Published online by Cambridge University Press

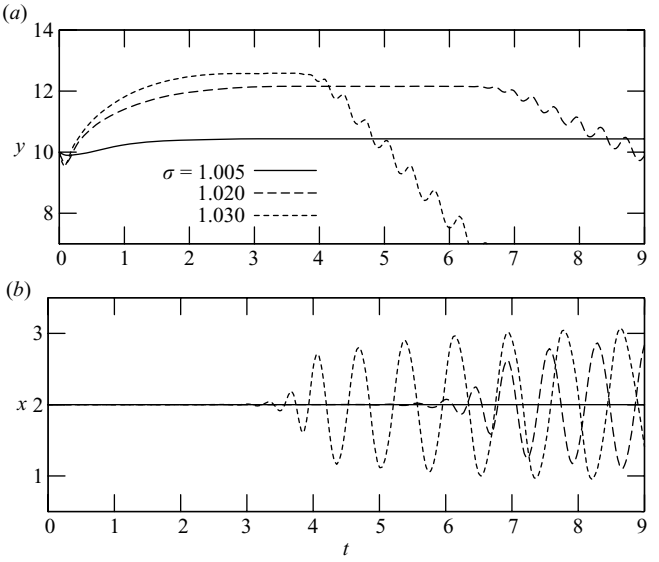


FIGURE 6. (*a*) Vertical and (*b*) horizontal position of a hot heavy particle for different values of σ. For $\sigma = 1.005$ $Gr_0 = 28$, for $\sigma = 1.02$ $Gr_0 = 110.2$ and for $\sigma = 1.03$ $Gr_0 = 170.5$.

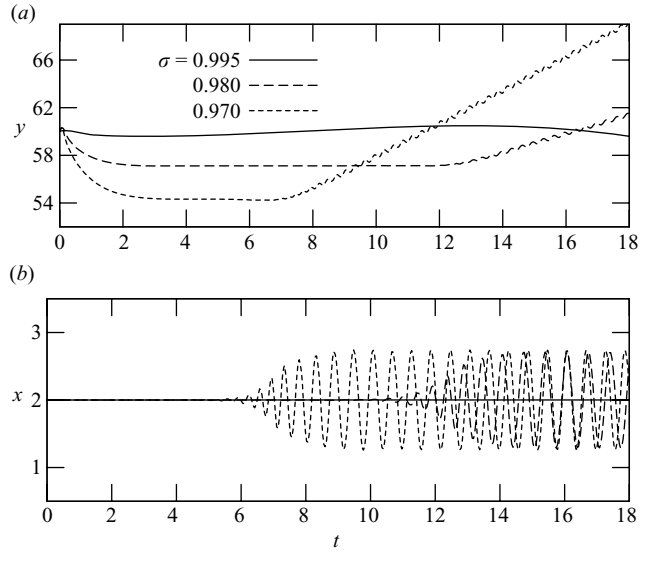


FIGURE 7. (*a*) Vertical and (*b*) horizontal position of a cold light particle for different values of σ. For $\sigma = 0.995$ $Gr_0 = -28.2$, for $\sigma = 0.98$ $Gr_0 = -114.5$ and for $\sigma = 0.97$ $Gr_0 = -185$.

is found for a cold light particle as we show in figure 7. Thermal levitation is stable for $\sigma = 0.995$ and unstable for smaller values of σ.

The trajectory of a particle with $\sigma = 1.02$ and $Gr = 110.2$ is shown in figure 8(*a*). The starting point is (2, 10). The particle initially sinks vertically, then floats and levitates near (2, 12). This can also be seen in figures 6(*a*) and 6(*b*). For $t > t_o$ the particle begins to oscillate first horizontally and then also vertically with twice the frequency, sinking and reaching the bottom of the cavity. The trajectory of a light

https://doi.org/10.1017/S0022112008001894 Published online by Cambridge University Press

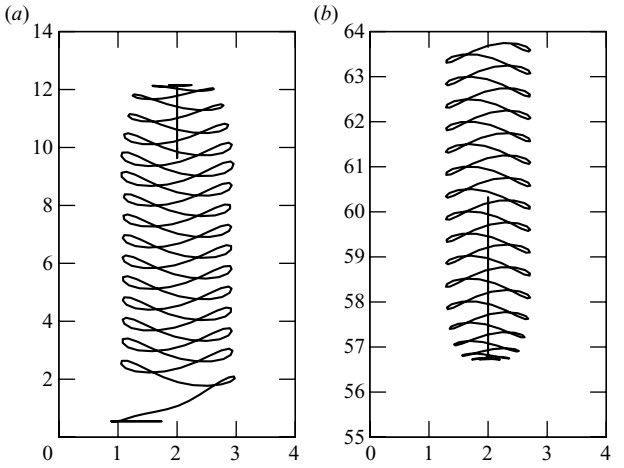


FIGURE 8. Particle trajectory: (*a*) hot particle $\sigma = 1.02$ and $Gr_0 = 110.2$; (*b*) cold particle $\sigma = 0.98$ and $Gr_0 = -114.8$.

particle is similar as we show in figure 8(*b*). The initial position is (2, 60). During the first instants the particle floats, then sinks and levitates where it will remain for a long time until it starts to oscillate horizontally and then also vertically with twice the frequency as it floats to the top of the cavity.

5. Conclusions

We used a two-component lattice Boltzmann equation to numerically study thermal levitation of a particle immersed in a fluid. A particle in a fluid levitates thermally when the convective force equals the buoyancy force, as described by (4.4). Once $C^{(\pm)}$ are known, given σ, we find Gr_0, the Grashof number for thermal levitation. Thermal levitation is stable whenever $Gr_c^{(-)} < Gr_0 < Gr_c^{(+)}$ and is unstable otherwise. The values of $C^{(\pm)}$ and $Gr_c^{(\pm)}$ were determined numerically by finding the hydrodynamic force on a fixed particle. We also found a Hopf supercritical bifurcation from steady to unsteady thermal levitation.

We acknowledge G. Barrios, J. J. Feng and G. Huelsz for fruitful suggestions. F.M. acknowledges the Dirección General de Asuntos del Personal Académico of the UNAM for the grant received during his post doctoral scholarship. Partial economic support from project CONACyT 25116 is also acknowledged.

REFERENCES

AIDUN, C. & LU, Y. 1995 Lattice-Boltzmann simulation of solid particles suspended in fluid. *J. Statist. Phys.* **81**, 49–61.

AIDUN, C., LU, Y. & DING, E. 1998 Direct analysis of particulate suspensions with inertia using the discrete Boltzmann equation. *J. Fluid Mech.* **373**, 287–311.

BÉRGE, P., POMEAU, Y. & VIDAL, C. 1988 *L'Ordre Dans le Chaos*. Hermann.

DESRAYAUD, G. & LAURIAT, G. 1993 Unsteady confined buoyant plumes. *J. Fluid Mech.* **257**, 617–646.

FENG, J., HU, H. H. & JOSEPH, D. D. 1994 Direct simulation of initial value problems for the motion of solid bodies in a Newtonian fluid. Part 1. Sedimentation. *J. Fluid Mech.* **261**, 95–134.

GAN, H., CHANG, J., FENG, J. & HU, H. 2003 Direct numerical simulation of the sedimentation of solid particles with thermal convection. *J. Fluid Mech.* **481**, 385–411.

https://doi.org/10.1017/S0022112008001894 Published online by Cambridge University Press

Guo, Z. & Zheng, C. 2002 An extrapolation method for boundary conditions in lattice Boltzmann method. *Phys. Fluids* **14**(6), 2007–2010.

Hu, H. H., Fortes, A. F. & Joseph, D. D. 1992*a* Experiments and direct simulation of fluid particle motion. *Video J. Engng Res.* **2**, 17–24.

Hu, H. H., Joseph, D. D. & Crochet, M. J. 1992*b* Direct simulation of fluid particle motion. *Theoret. Comput. Fluid Dyn.* **3**, 285–306.

Huang, H., Lee, T. S. & Shu, C. 2006 Thermal curved boundary treatment for the thermal lattice Boltzmann equation. *Intl J. Mod. Phys.* C **17**(5), 631–643.

Inamuro, T., Yoshino, M. M., Inoue, H., Mizuno, R. & Ogino, F. 2002 A lattice Boltzmann method for a binary miscible fluid mixture and its application to a heat-transfer problem. *J. Comput. Phys.* **179**, 201–215.

Ladd, A. J. C. 1994 Numerical simulations of particulate suspensions via a discretized Boltzmann equation. Part 1. Theoretical foundation. *J. Fluid Mech.* **271**, 285–309.

Mei, R., Yu, D., Shyy, W. & Luo, L. 2002 Force evaluation in the lattice Boltzmann method involving curved geometry. *Phys. Rev.* E **64**, 041203.

Ottino, J. M. 1989 *The Kinematics of Mixing: Stretching, Chaos and Transport*. Cambridge University Press.

Qian, Y., d'Humieres, D. & Lallemand, P. 1992 Lattice BGK models for the Navier–Stokes equation. *Eur. Phys. Lett.* **17**, 479–484.

Sadat, H. & Couturier, S. 2000 Performance and accuracy of a meshless method for laminar natural convection. *Numer. Heat Transfer* B **37**, 455–467.

Shan, X. 1997 Simulation of Rayleigh–Bénard convection using a lattice Boltzmann method. *Phys. Rev.* E **55**(3), 2780–2788.

Shu, C. & Zhu, Y. D. 2002 Efficient computation of natural convection in a concentric annulus between an outer square cylinder and an inner circular cylinder. *Intl J. Numer. Meth. Fluids* **38**, 429–445.

Yu, Z., Shao, X. & Wachs, A. 2006 A fictitious domain method for particulate flows with heat transfer. *J. Comput. Phys.* **217**, 424–452.

https://doi.org/10.1017/S0022112008001894 Published online by Cambridge University Press